Applied Catalysis B: Environmental 84 (2008) 142–147

Contents lists available at ScienceDirect

Applied Catalysis B: Environmental

journal homepage: www.elsevier.com/locate/apcatb

Synthesis of effective titania nanotubes for wastewater purification

Han-Jun Oh [a,*], Jong-Ho Lee [b], Young-Jig Kim [c], Su-Jeong Suh [c], Jun-Hee Lee [d], Choong-Soo Chi [e]

[a] Department of Materials Science, Hanseo University, Seosan 352-820, Republic of Korea
[b] Department of Chemistry, Hanseo University, Seosan 352-820, Republic of Korea
[c] Department of Metallurgical Engineering, Sungkyunkwan University, Suwon 440-746, Republic of Korea
[d] Department of Materials Science and Engineering, Donga University, Busan 604-714, Republic of Korea
[e] School of Advanced Materials Engineering, Kookmin University, Seoul 136-702, Republic of Korea

ARTICLE INFO

Article history:
Received 13 July 2007
Received in revised form 11 March 2008
Accepted 20 March 2008
Available online 30 March 2008

Keywords:
Titania nanotube
Anodization
Anatase
Aniline blue
Photocatalyst

ABSTRACT

In order to synthesize a self-organized, TiO_2 nanotubular layer for wastewater purification, anodizations were performed at constant applied potential in hydrofluoric acid and the anodic TiO_2 layer was heat treated. The anodic nanotube arrays were also influenced by the applied anodic potentials and HF concentrations. The anodic TiO_2 nanotubular structured film with various morphologies and crystal structures can be synthesized by proper electrochemical anodization and additional annealing treatment. The photocatalytic efficiencies were maximized for the anatase-type, TiO_2 nanotubular layer which was prepared by annealing at 550 °C.

1. Introduction

Recently many studies have investigated titanium dioxides (TiO_2) due to their varieties of functional properties. Especially, TiO_2 nanotube structure has attracted considerable interest because of its large surface area and potential technological applications such as biomaterial [1], gas sensor, and photocatalysis [2,3]. In general, the self-organized nanotubular layer [4–6] can be achieved at anodic potential range lower than 40 V, but to maximize the wide applications for the titania nanotubes with various functional properties, the characteristics of TiO_2 nanotubes, including microstructure, crystallinity, and film thickness, need to be investigated. However, there are few reports of these synthesis parameters. In this study, therefore, the TiO_2 nanotubes with functional properties were synthesized by anodic oxidation in hydrofluoric (HF) solution. To investigate the fabrication parameters of the titania nanotubes, we examined the effects of applied anodic potential and electrolyte concentration on the formation of self-organized anodic TiO_2 nanotubes. Because the anodic TiO_2 nanotube prepared in HF electrolyte has not only a high chemical stability but also the advantage of a high specific surface area, it can be applied to photocatalysts for the degradation of organic pollutants in aqueous media. Among photocatalysts, the photocatalytic efficiency of the anatase-type TiO_2 crystal structure is known to be more effective than that of other crystal structures. However, the anodic nanotubular film consists of an amorphous TiO_2 structure. To transform the crystal structure, the anodic titania films were annealed at 450, 550, and 650 °C for 1 h, and the photocatalytic efficiency was investigated.

2. Experimental

The substrate used was a commercial grade, pure titanium plate (99.6 wt.%). After the titanium specimens were pretreated and degreased in *n*-hexane, the anodic titania nanotubes were synthesized by anodization in HF solutions at a constant potential. The crystalline structure on the anodic TiO_2 layer was characterized by X-ray diffraction (XRD; Philips, Model PW1710). The microstructures on the anodic TiO_2 nanotubes were observed using a field emission scanning electron microscope (FE-SEM, Philips XL30 ESEM-FEG). To investigate the light absorption properties of titania films, analysis of reflectance absorption spectra was performed using a UV–vis spectrophotometer (Cary 500 Scan UV–vis–NIR spectrophotometer) with a wavelength range of 250–550 nm.

The dye and dichloroacetic acid (DCA) decomposition rates of the anodic TiO_2 film were evaluated using a Pyrex glass reactor with a diameter of 70 mm and a height of 20 mm at 25 °C. The apparent geometrical irradiation area of the TiO_2 specimens as the

* Corresponding author.
E-mail address: hanjun58@hanseo.ac.kr (H.-J. Oh).

0926-3373/$ – see front matter © 2008 Elsevier B.V. All rights reserved.
doi:10.1016/j.apcatb.2008.03.014

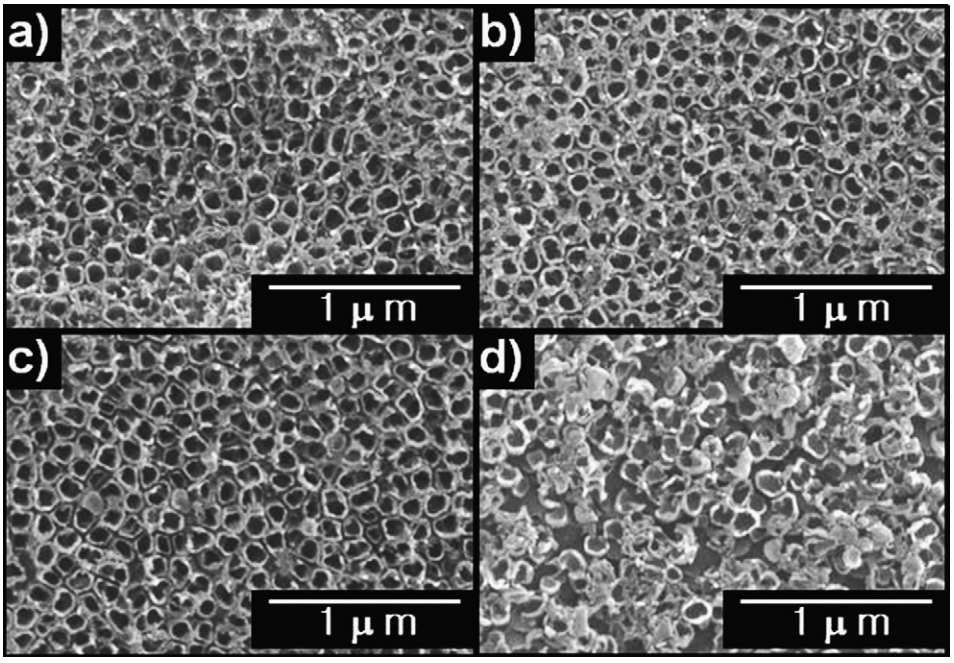

Fig. 1. Morphologies of self-organized nanotube arrays on anodic titania. The anodic TiO_2 nanotube films formed at 20 V in 0.5 wt.% (a), 1.0 wt.% (b), 2.0 wt.% (c), and 3.0 wt.% (d) HF solution.

photocatalyst was 10.5 cm^2. For the photocatalytic experiment, 83 μM aniline blue solution (Fulka, pH 4) and 0.48 mM DCA (Aldrich, 99%, pH 5.7) solutions were prepared. All of the experiments for photocatalytic reaction were performed with 30 mL solution and using a 100 W Hg lamp as the light source. UV–vis spectroscopy (Unicam 8700) was performed to determine the decomposition rate of the dye at the absorption band of 600 nm. Dichloroacetic acid decomposition rate was carried out using a Total Organic Carbon (TOC) analyser (Shimadzu 5000) with a combustion/non-dispersive infrared gas analysis method.

3. Results and discussion

3.1. Effects of electrolytes

In order to investigate the effect of HF solution concentration on the self-organized nanotubular structure in anodic titania film, the

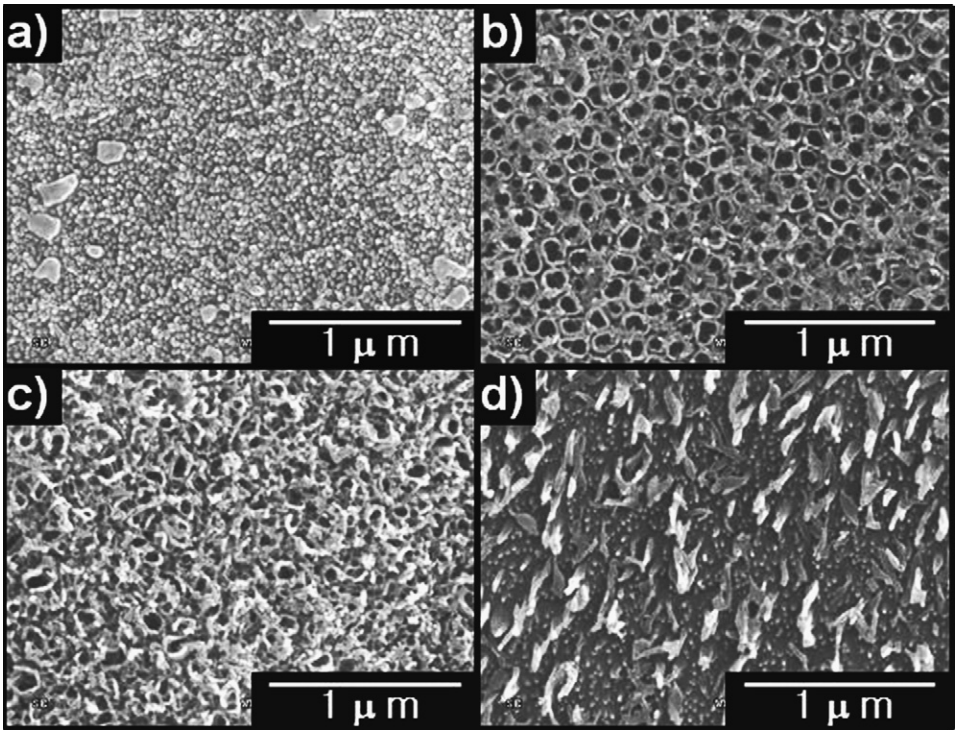

Fig. 2. Nanotubular arrays in anodic titania prepared by anodization in 2 wt.% HF solution for 40 min at 15 V (a), 20 V (b), 25 V (c), and 40 V (d).

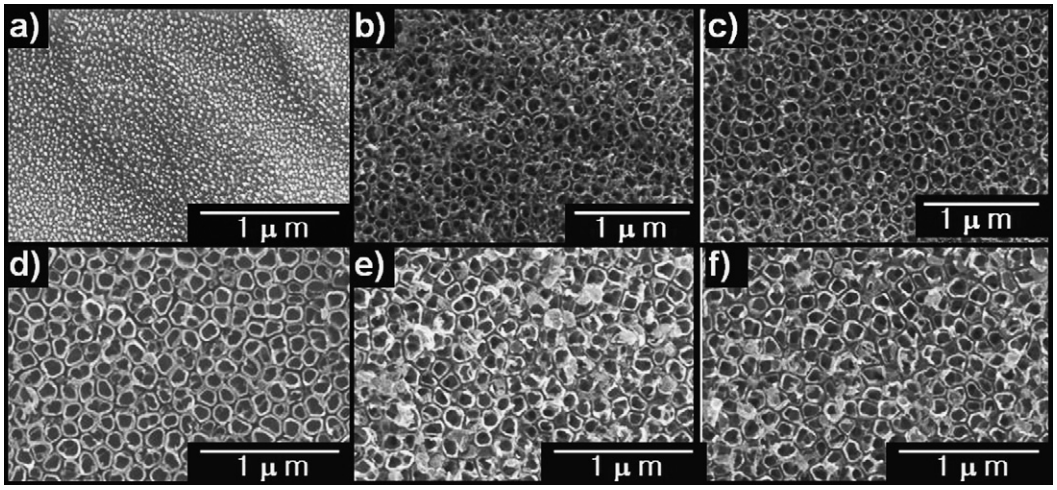

Fig. 3. FE-SEM images of the top view of the anodic titania layer after anodization at 20 V in 2.0 wt.% HF solution for 1 min (a), 10 min (b), 20 min (c), 40 min (d), 120 min (e), and 180 min (f).

anodizations were performed at a constant applied potential of 20 V for 40 min in 0.5, 1.0, 2.0, and 3.0 wt.% HF electrolytes. Fig. 1 shows the self-organized nanotube arrays on anodic titania formed in HF solution. In the HF solution concentration less than 2.0 wt.%, no significant change of pore arrangements and microstructure of the anodic TiO_2 nanotubular layer was detected, whereas for high concentration HF solution, for example 3.0 wt.%, the morphologies of the self-organized nanotubular layer changed to an irregular arrangement. Therefore, it can be expected that the regularity of the nanotube arrangement on the anodic titania layer increased with increasing HF acid concentration, up to a maximum, and then gradually decreased. In an anodic process it is well known that the growth of the anodic oxide film arises from a competition between dissolution due to acidic solution and film growth due to anodic reaction. As shown in Fig. 1, because the dissolution process is facilitated in 3.0 wt.% HF electrolyte, the nanotubular arrays undergo irregular change. The regular nanotubular arrays can be obtained from an anodization in a concentration range lower than 3.0 wt.% HF electrolyte at 20 V.

3.2. Effects of anodic potentials

To observe the effects of applied anodic potentials on the self-organized nanotube arrays, the anodizations were performed in 2.0 wt.% HF solution at 15, 20, 25, and 30 V for 40 min. Fig. 2 shows that the applied anodic potential clearly affected the regular nanotube arrangements and surface morphologies on the anodic titania films. At a low anodic potential range (e.g. Fig. 2a), the arrangement of the self-organized nanotube was irregular and unstable, whereas a higher applied potential facilitated the

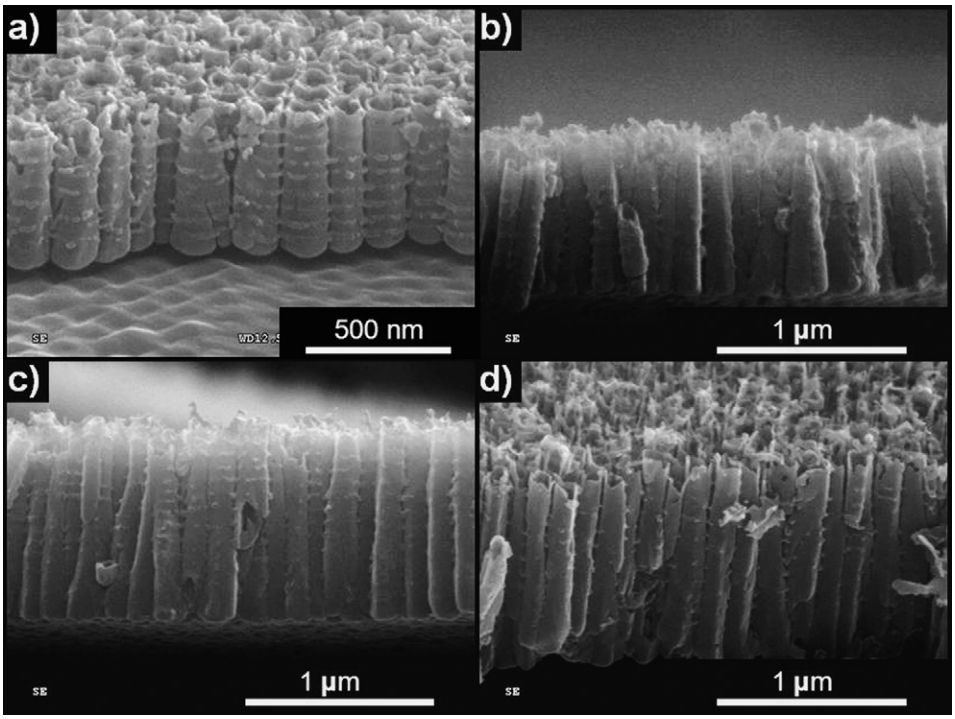

Fig. 4. FE-SEM cross-sectional images with anodic time in 2.0 wt.% HF solution at 20 V for (a) 40 min, (b) 60 min, (c) 120 min, and (d) 180 min.

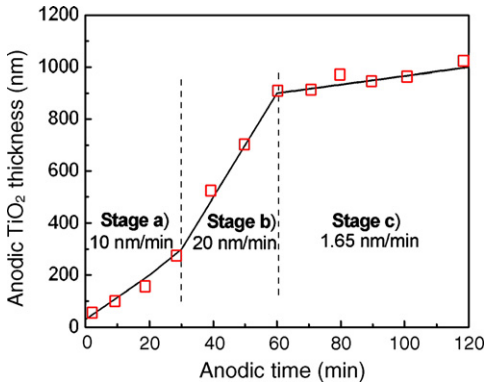

Fig. 5. Growth rate of the anodic TiO_2 nanotubular layer with anodic time. The anodization was performed in 2.0 wt.% HF solution at 20 V.

formation process of anodic titania nanotubes, up to 20 V, after which the arrays of the self-organized nanotubes became stable and gradually changed to a regular pattern. Meanwhile, at the higher anodic potential of more than 20 V at which the nanotube arrays reached an optimum, the morphologies of the self-organized nanotubular layer [7] became irregular again. The best array of titania nanotubes was obtained under an anodic potential of 20 V in 2 wt.% HF solution, as represented in Fig. 2.

3.3. Effects of anodic time

To observe the surface morphology of the anodic TiO_2 layer, a constant anodic current of 1.8 A was applied on the titanium surface in 2.0 wt.% HF, and then the anodic potential was increased slowly. When the anodic potential reached 20 V, the anodizing process was carried out at a constant potential of 20 V. The variations of surface morphology of the anodic titania during the anodizing process are exhibited in Fig. 3. In the early stage of anodization, as seen in Fig. 3a, the anodic TiO_2 layer was unstable, and no tubular structure was initially observed. After an anodic time of 10 min, a tubular morphology was observed on the titania surface, but the porous tubular structure was less uniform and the distributions were more scattered. For anodic times more than 10 min, the morphology of the self-organized nanotubes became stable and gradually changed to a regular pattern, but beyond 180 min, the morphology became irregular again. The cross-sectional images of the TiO_2 nanotubular layer with anodic time are represented in Fig. 4.

The growth rate of the anodic titania nanotubular layer with anodic time can be represented in three stages, as shown in Fig. 5. In the initial anodization, the growth rate of the anodic titania was retarded, indicating an average growth rate of 10 nm/min. In the period between 30 and 60 min, the growth rate increased linearly to 20 nm/min. For the applied anodic time of more than 60 min, the growth rate decreased to 1.65 nm/min. In the early anodizing stage (stage a), a barrier and compact titania [8] were formed on the titanium substrate, which may have decreased the growth rate in this stage compared to that of porous titania films with low density. In the second stage, a breakdown of the compact titania layer occurred on the surface, after which a porous TiO_2 layer gradually grew and the titania film layer was thickened. This stage exhibited a fast increase of growth rate, and a regular nanotubular morphology was obtained. The decrease of growth rate in the third stage (stage c) compared to the second stage (stage b) may be explained by a competition of conditions leading to the formation of an anodic nanotubular layer during the anodic process and conditions leading to the dissolution of the anodic titania tubular films in acidic electrolyte. With increasing thickness, the growth rate of the anodic titania films decreased and the dissolution rate increased. Therefore, the growth rate of the TiO_2 nanotubular layer exhibited a lower ratio than that of stage b.

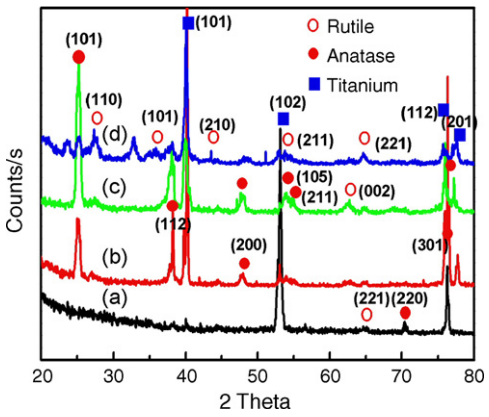

Fig. 6. XRD results of anodic titania nanotube films as anodized (a), and with 1-h heat treatment at 450 °C (b), 550 °C (c), and 650 °C (d).

3.4. Effects of heat treatment of anodic titania film

In order to investigate the effects of heat treatment on the crystal structure, the anodic titania nanotube films were heat treated at 450, 550 and 650 °C for 1 h, and the crystalline structure was examined. Fig. 6 shows the XRD results for the anodic titania films with and without heat treatment. The XRD result of the anodic titania film without heat treatment, as shown in Fig. 6, indicated the presence of titanium, anatase, and rutile peaks. The titanium peaks originated from the Ti substrate, while the anatase and rutile peaks were weakly presented and were not clear, indicating that crystalline titania structure was only slightly produced in anodized TiO_2 nanotube films. For anodic TiO_2 film annealed at 450 °C, the anatase-type crystalline TiO_2 peaks increased gradually. At 550 °C annealing, the anatase peaks became more numerous and strong, whereas at 650 °C the crystalline phase of rutile-type peaks was observed more than that of the anatase phase. As can be seen in Fig. 6, various crystal structures of anodic TiO_2 nanotubular film were obtainable with additional annealing treatment.

3.5. Absorbance response of titania films

The UV–vis diffuse reflectance absorption spectra of anodized nanotubular titania films are shown in Fig. 7. As seen from Fig. 7,

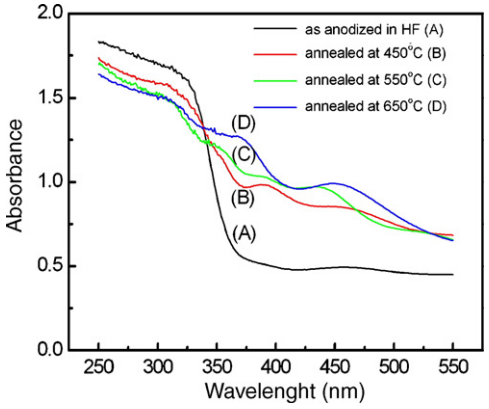

Fig. 7. UV–vis diffuse reflectance absorption spectra of anodized TiO_2 nanotubular film without annealing (A), annealed at 450 °C (B), 550 °C (C), and 650 °C (D).

there are some differences of absorbance response between non-annealed and annealed titania film. However, there are no significant differences of the absorption properties among the annealed films in UV and visible light region.

The absorbance response of non-annealed titania film (Fig. 7(A)) exhibits lower adsorption in visible light region, whereas the annealed TiO_2 films show a red-shift and stronger absorption in the range of wavelength from 350 to 550 nm. The absorbance responses can be explained in terms of surface color and crystalline structure of titania film. The color of annealed titania film was yellowish with heat treatment at 450 °C, blue at 550 °C and dark brown at 650 °C, respectively. However, the color of anodic TiO_2 film without heat treatment was bright white. This causes more adsorption in the ultra violet region and reflection in visible light region than that of titania films with heat treatment. In the case of TiO_2 film annealed at 450 °C, as shown in Fig. 7(B), the adsorption onset around 380 nm was observed, which was probably caused by increasing the anatase-type crystalline TiO_2 during annealing. The TiO_2 film annealed at 550 °C (Fig. 7(C)) showed a slight red-shift related to increasing the anatase ratio, and an absorption peak was observed at 450 nm, which was mainly attributed to the light adsorption of blue color on titania film. However, for TiO_2 film annealed at 650 °C, the position of the absorption onset was observed around 420 nm, as phase transition of anatase into rutile phase takes place and ratio of rutile phase increases. The wavelength of 420 nm means that energy of band gaps for the anodic TiO_2 films annealed at 650 °C represent about 3.0 eV. The UV–vis spectra in Fig. 7 are consistent with the changes in crystalline structure observed with the X-ray diffractometer in Fig. 6.

3.6. Efficiency of photocatalytic reaction

Fig. 8 shows the photocatalytic efficiency of the anodic TiO_2 nanotubular films with or without heat treatment for dye decomposition with irradiation by Hg lamp. Before the experiment, the starting solution was adjusted to 83 μM aniline blue for decomposition efficiency and the pH was kept constant at 4.0 through the experiment. In order to obtain the actual photocatalytic efficiency of the prepared catalysts, the blank tests without anodic TiO_2 catalysts were carried out under Hg lamp irradiation and a small degradation of aniline blue occurred due to Hg lamp irradiation. This value was compensated during evaluation of photocatalytic efficiency. After dye decomposition test for 3 h, from the photocatalytic reaction on the anodic TiO_2 film without heat treatment, 12.2% of the dye was removed after 1 h, and 25.4% after 3 h. The corresponding dye removal rates for the heat-treated anodic TiO_2 films were 21.8% and 39.7% with heat treatment at 450 °C, 44.5% and 85.9% at 550 °C, and 21.8% and 44.5% at 650 °C, respectively. However, as shown in Fig. 8, the dye degradation rate decreased with increasing annealing temperature above 550 °C.

Table 1
The reaction rate of dye decomposition after irradiation for 1 h on anodic TiO_2 nanotube layer heat treated at 550 °C for 1 h

Specimen	Initial dye concentration (μM)	Resultant concentration after 1 h (μM)	Initial rate [μmol L^{-1} s^{-1}]
TiO_2 annealed at 550 °C for 1 h.	1.66	0.69	2.722×10^{-4}
	3.32	1.43	5.306×10^{-4}
	4.98	2.06	8.194×10^{-4}
	6.64	3.17	9.750×10^{-4}

The photocatalytic reaction order and the rate constant on these TiO_2 specimens can be calculated using Eq. (1).

$$\text{Reaction rate}[\text{mol}\,\text{L}^{-1}\ \text{s}^{-1}] = \frac{-\text{d}[A]}{\text{d}t} = k[A]^x, \quad (1)$$

where $[A]$ is the concentration of reactant, x is the reaction order, and k is the rate constant. In order to determine the reaction order, the dye decomposition rates on anodic TiO_2 nanotube film annealed at 550 °C are summarized in Table 1.

As the initial concentration of aniline blue increases from 1.66 to 6.64 μM, the initial rate after 1 h of Hg lamp irradiation increases from 2.722×10^{-4} to 9.750×10^{-4} μM/s, and the initial rate increased with the same ratio with respect to the concentration of aniline blue. These indicate that the reaction order for the dye decomposition is first dimension. The kinetics of photocatalytic reactions for TiO_2 catalysts have been reported by several research groups [9–12], and were also explained in terms of first order reaction rate [13–16]. Therefore, the kinetic constants during the degradation of aniline blue can be calculated by first order reaction rate, and the change of concentration with reaction time can be written as Eq. (2),

$$-\frac{\text{d}C}{\text{d}t} = k \times C, \quad (2)$$

where the C is dye concentration in solution. From the Eq. (2) kinetic constant can be expressed as Eq. (3)

$$\ln\frac{C_0}{C_t} = kt, \quad (3)$$

where C_0 represents the initial concentration and C_t is resultant concentration of dye after photocatalytic reaction time. The

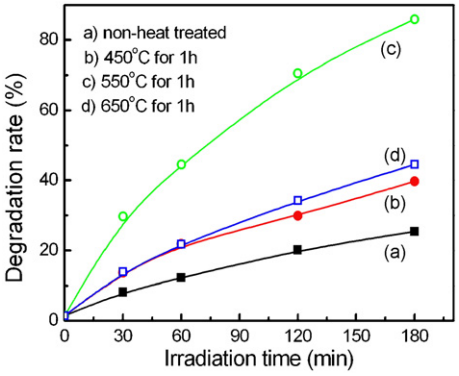

Fig. 8. Photocatalytic degradation rate of aniline blue on anodic TiO_2 tubular layer with geometric surface of 10.5 cm^2 in 83 μM aniline blue solution.

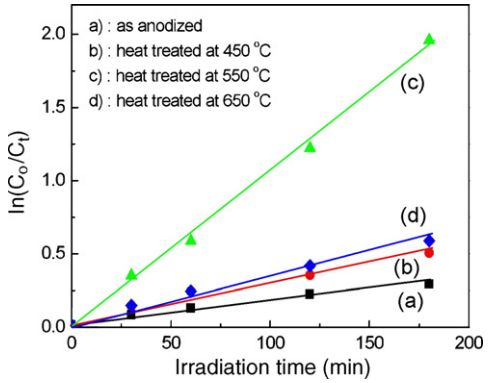

Fig. 9. Dependence of $\ln(C_0/C_t)$ vs. time (min) for aniline blue decomposition on TiO_2 nanotubular films.

Table 2
Rate constants of aniline blue degradation on anodic TiO_2 nanotubular layers and linear regression coefficients calculated from Fig. 9

Anodic TiO_2 nanotublar catalyst	Rate constant, k (min^{-1})	R^2
As anodized TiO_2	0.00152	0.9863
TiO_2 annealed at 450 °C	0.00258	0.9765
TiO_2 annealed at 550 °C	0.01066	0.9964
TiO_2 annealed at 650 °C	0.00311	0.9930

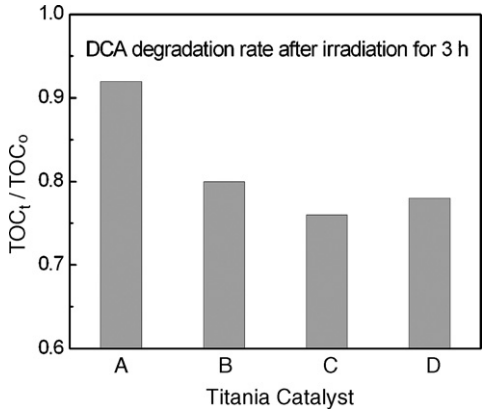

Fig. 10. Photocatalytic degradation of DCA (C_0 = 0.48 mM, initial pH 5.7) on the anodic titania catalyst films as anodized (A), and with 1-h heat treatment at 450 °C (B), 550 °C (C), and 650 °C (A).

relationship between $\ln(C_0/C_t)$ and photocatalytic reaction time is illustrated in Fig. 9. The rate constants for the degradation of the aniline blue on anodic TiO_2 catalysts have been evaluated and presented in Table 2. From Figs. 8 and 9 and Table 2, the titania nanotubular photocatalyst annealed at 550 °C shows much higher efficiency and activity of dye degradation than the other catalysts do. This high efficiency may be attributed to the crystal structures of the anodic TiO_2 nanotubular film. As can be seen in Fig. 6, the various crystal structures of the anodic TiO_2 nanotubular film were obtained by additional annealing treatment, and the anatase structure was increased after heat treatment at 550 °C. This suggests that anatase-type, crystalline TiO_2 in anodic, nanotubular titania film plays a significant role in the photocatalytic reaction.

Fig. 10 shows the result of the degradation reaction of the dichloroacetic acid (DCA) after irradiation of 3 h. Before evaluating the DCA decomposition rates, the blank tests were performed and net changes of the TOC content were compensated. As shown in Fig. 10, 8.4% of the DCA (measured by TOC amount) was removed from the photocatalytic reaction on the anodic TiO_2 film without annealing treatment. The corresponding DCA decomposition rates for the heat-treated anodic TiO_2 films were 19.1% with heat treatment at 450 °C, 23.6% at 550 °C and 21.8% at 650 °C, respectively. As shown in Fig. 10, the anodic TiO_2 film annealed at 550 °C shows much higher DCA degradation rate and the photocatalytic activities of titania catalysts are very similar for dye decomposition.

4. Conclusions

In order to synthesize a self-organized, TiO_2 nanotubular layer for wastewater purification, anodizations were performed in HF electrolyte. In addition, the effects of heat treatment on the crystal structure in the synthesized titania films and the photocatalytic efficiencies were investigated.

With an applied potential of 20 V, regular nanotubular arrays were obtained by anodization in HF electrolyte at a concentration range lower than 3.0 wt.%. The anodic nanotube arrays were also influenced by the applied anodic potentials, and the best array of titania nanotubes was achieved under an anodic potential of 20 V in 2.0 wt.% HF solution. The XRD results of the anodic TiO_2 nanotubular films indicated very weak and unclear anatase and rutile peaks for the anodized titania films without heat treatment. This suggests that crystalline TiO_2 is only slightly produced by anodization. After annealing at 550 °C for 1 h, the intensity of the anatase peaks increased and strengthened, whereas at 650 °C the rutile-type crystalline phase surpassed the anatase phase. The results indicated that anodic TiO_2 nanotubular films with various morphologies and crystal structures can be synthesized by proper electrochemical anodization and additional annealing treatment, which can be tailored to produce a titania nanotubular film with high functional properties. From the photocatalytic results, the anodic titania photocatalyst heat treated at 550 °C exhibited the highest efficiency of dye and dichloroacetic acid (DCA) degradation among the catalysts. This high efficiency of the catalytic reaction may be attributed to the predominant presence of the anatase-type structure in the anodic film.

References

[1] J.-H. Lee, S.-E. Kim, Y.-J. Kim, C.-S. Chi, H.-J. Oh, Mater. Chem. Phys. 98 (2006) 39.
[2] M. Adachi, Y. Murata, S. Yoshikawa, Chem. Lett. 8 (2000) 942.
[3] J.-H. Lee, H.-J. Oh, Y. Jeong, Y.-J. Lee, J.-S. Kim, C.-S. Chi, Mater. Sci. Forum 475–479 (2005) 4153.
[4] J.M. Macak, H. Tsuchiya, P. Schmuki, Angew. Chem. Int. Ed. 44 (2005) 2100.
[5] J.M. Macak, H. Tsuchiya, L. Taveira, S. Aldabergerova, P. Schmuki, Angew. Chem. Int. Ed. 44 (2005) 7463.
[6] K. Shankar, G.K. Mor, A. Fitzgerald, C.A. Grimes, J. Phys. Chem. C 111 (2007) 21.
[7] H. Li, X. Bai, Y. Ling, J. Li, D. Zhang, J. Wang, Electrochem. Solid-State Lett. 9 (2006) B28.
[8] L.V. Taveira, J.M. Macak, K. Sirotna, L.F.P. Dick, P. Schmuki, J. Electrochem. Soc. 152 (2005) B405.
[9] N.R.C.F. Machado, V.S. Santana, Catal. Today 107 (2005) 595.
[10] J. Medina-Valtierra, E. Moctezumab, M. Sanchez-Cardenas, C. Frausto-Reyes, J. Photochem. Photobiol. A 174 (2005) 246.
[11] D. Vione, C. Minero, V. Maurino, M.E. Carlotti, T. Picatonotto, E. Pelizzetti, Appl. Catal. B 58 (2005) 79.
[12] C. Wu, X. Liu, D. Wei, J. Fan, L. Wang, Water Res. 35 (2001) 3927.
[13] J.-M. Herrmann, H. Tahiri, Y. Ait-Ichou, G. Lassaletta, A.R. Gonzalez-Elipe, A. Fernandez, Appl. Catal. B 13 (1997) 219.
[14] K.-H. Wang, Y.-H. Hsieh, M.-Y. Chou, C.-Y. Chang, Appl. Catal. B 21 (1999) 1.
[15] S.N. Hosseini, S.M. Borghei, M. Vossoughi, N. Taghavinia, Appl. Catal. B 74 (2007) 53.
[16] B. Zielińska, A.W. Morawski, Appl. Catal. B 55 (2005) 221.